Supplementary Material: A Unified Degradation-Robust Approach to SSL and UDA for 3D Medical Images

Anonymous submission

A More Details of Datasets and Implementation

Left Atrial Segmentation Challenge (LA) dataset : The LA dataset (Xiong et al. 2021) contains 100 3D gadolinium-enhanced MR scans and LA segmentation masks for training and validation. In line with (Wang and Li 2024; Su et al. 2024), 80 scans are used for training and 20 for evaluation. We follow the same preprocessing steps as in the previous study (Wu et al. 2022), where the training volumes are randomly cropped to a size of $112 \times 112 \times 80$ as the model's input. During training, the labeled dataset is used for validation to select the best model.

Pancreas-CT Dataset : The Pancreas-CT dataset (Clark et al. 2013) contains 82 3D abdominal contrast-enhanced CT scans, each with a fixed resolution of 512 × 512 pixels and varying thickness from 1.5 to 2.5 mm. We crop the CT images around the pancreatic region and apply a soft tissue CT window of $[-120, 240]$ HU, following the methodology of (Wu et al. 2022). Among these, 62 scans are used for training, with performance evaluated on the remaining 20. During training, the volumes are randomly cropped to dimensions of $96 \times 96 \times 96$. During training, the labeled dataset is used for validation to select the best model.

MMWHS Dataset : The Multi-Modality Whole Heart Segmentation Challenge 2017 dataset (MMWHS) (Zhuang and Shen 2016) includes images from two modalities, MR and CT, used for cardiac segmentation, with no pairwise relationship between the modalities. Following earlier research (Wang and Li 2024), we focus on four heart structures: the left ventricular blood cavity (LVC), the ascending aorta (AA), the left atrium blood cavity (LAC), and the left ventricle myocardium (MYO). We maintain the test set identical to previous studies to ensure a fair comparison.

The hyper-parameters for different datasets are shown in Table 1.

Dataset	Patch Size	Learning Rate	Batch Size	Feature Size (F)	β
LA	112 × 112 × 80	1e-2	4	32	10
Pancreas	96 x 96 x 96	1e-2	4	32	4
MMWHS	128 × 128 × 128	5e-3	2	32	10

Table 1: Details of the datasets, including their respective patch sizes, learning rates, batch sizes, feature sizes, and the parameter β.

B Visualization Results

Additional qualitative results of our method on degraded images are provided in Figure 1. This figure illustrates a comparison of visualization results between our method and the state-of-the-art approach (GenericSSL) on the MMWHS dataset in the MR to CT setting for degraded images. Our approach demonstrates superior performance even when dealing with noisy images.

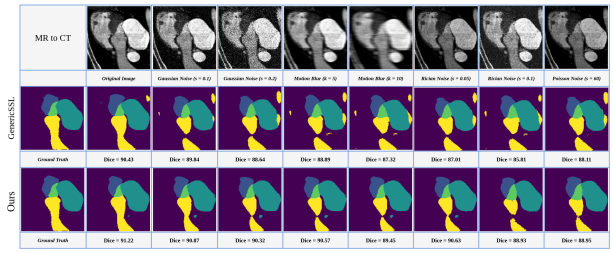

Figure 1: Comparison of visualization results between our approach and the SOTA approach (GenericSSL) on the MMWHS dataset in the MR to CT setting for degraded images. The second row presents the outcomes of Genericssl approach, while the third row shows the outcomes of our approach.

C Preprocessing Techniques for Image Denoising

Gaussian Noise: To address Gaussian noise, we first apply a Gaussian filter (Gonzalez 2009) with a standard deviation (σ) of 0.1 to reduce noise. However, relying solely on the Gaussian filter isn't sufficient, as it may not effectively remove outliers. Therefore, we follow this with a median filter (Gonzalez 2009) of size 3 to eliminate any remaining outliers, further enhancing image quality. This combination ensures a more robust noise reduction compared to using only a Gaussian filter.

Motion Blur: We use the Richardson-Lucy deconvolution algorithm (RLD) (Richardson 1972; Lucy 1974) to remove motion blur from the images. This algorithm iteratively refines the image using a specified point spread function (PSF) that models the motion blur's shape and direction.

The noise-to-signal ratio (NSR) is set to 0.01 to balance the deconvolution process and reduce noise, improving image sharpness. The algorithm is run for 15 iterations.

Rician and Poisson Noise: To address Rician and Poisson noise, we apply anisotropic diffusion (Perona and Malik 1990) during preprocessing. This method smooths the image while preserving important structures and edges. By diffusing the image in a way that minimizes the blurring of significant features, anisotropic diffusion effectively reduces noise and enhances image quality.

References

Clark, K.; Vendt, B.; Smith, K.; Freymann, J.; Kirby, J.; Koppel, P.; Moore, S.; Phillips, S.; Maffitt, D.; Pringle, M.; et al. 2013. The Cancer Imaging Archive (TCIA): maintaining and operating a public information repository. *Journal of digital imaging*, 26: 1045–1057.

Gonzalez, R. C. 2009. *Digital image processing*. Pearson education india.

Lucy, L. B. 1974. An iterative technique for the rectification of observed distributions. *Astronomical Journal, Vol. 79, p. 745 (1974)*, 79: 745.

Perona, P.; and Malik, J. 1990. Scale-space and edge detection using anisotropic diffusion. *IEEE Transactions on pattern analysis and machine intelligence*, 12(7): 629–639.

Richardson, W. H. 1972. Bayesian-based iterative method of image restoration. *JoSA*, 62(1): 55–59.

Su, J.; Luo, Z.; Lian, S.; Lin, D.; and Li, S. 2024. Mutual learning with reliable pseudo label for semi-supervised medical image segmentation. *Medical Image Analysis*, 103111.

Wang, H.; and Li, X. 2024. Towards generic semi-supervised framework for volumetric medical image segmentation. *Advances in Neural Information Processing Systems*, 36.

Wu, Y.; Ge, Z.; Zhang, D.; Xu, M.; Zhang, L.; Xia, Y.; and Cai, J. 2022. Mutual consistency learning for semi-supervised medical image segmentation. *Medical Image Analysis*, 81: 102530.

Xiong, Z.; Xia, Q.; Hu, Z.; Huang, N.; Bian, C.; Zheng, Y.; Vesal, S.; Ravikumar, N.; Maier, A.; Yang, X.; et al. 2021. A global benchmark of algorithms for segmenting the left atrium from late gadolinium-enhanced cardiac magnetic resonance imaging. *Medical image analysis*, 67: 101832.

Zhuang, X.; and Shen, J. 2016. Multi-scale patch and multi-modality atlases for whole heart segmentation of MRI. *Medical image analysis*, 31: 77–87.